Energy Reports 8 (2022) 7476–7487

Contents lists available at ScienceDirect

Energy Reports

journal homepage: www.elsevier.com/locate/egyr

Research paper

Experimental investigation and modelling of biodiesel combustion in engines with late direct injection strategy

José Antonio Vélez Godiño [a,*], Miguel Torres García [b], Francisco José Jiménez-Espadafor Aguilar [b]

[a] Departamento de Máquinas y Motores Térmicos, Escuela Superior de Ingeniería, Universidad de Cádiz. Avda. Universidad de Cádiz, n° 10, 11519, Puerto Real (Cádiz), Spain
[b] Departamento de Ingeniería Energética, Escuela Técnica Superior de Ingeniería, Universidad de Sevilla. Camino de los Descubrimientos, s/n, 41092, Seville, Spain

ARTICLE INFO

Article history:
Received 31 January 2022
Received in revised form 16 May 2022
Accepted 29 May 2022
Available online xxxx

Keywords:
Biofuels
Biodiesel
Brassica napus
Low-temperature combustion
Predictive model

ABSTRACT

The combination of alternate fuels, such as biodiesel, and low-temperature combustion (LTC) constitutes a promising solution to reduce pollutant emission and to avoid dependence on fossil fuels. However, this concept requires additional research to optimise LTC of biodiesel over wider operating ranges, specifically including the implementation of numerical models to assist in the development of these engines. In this work, an experimental analysis was carried out assessing both thermal performance and emissions derived from the LTC of diesel/biodiesel blends with late direct injection. Furthermore, this analysis allowed implementing a predictive tool to characterise in-cylinder pressure trace under this operation strategy. This model was coupled with an empirical law to simulate heat release during the combustion process. Least squares method was applied to fit this empirical law to experimental data involving different conditions in terms of percentages of rapeseed biodiesel in the fuel blend, rotational speed, fuel/air equivalence ratio and percentages of external exhaust gas recirculation. To build the predictive model, a multiple regression methodology was used to correlate the law parameters with the operating conditions. Finally, a validation process based on the simulation of in-cylinder pressure trace was developed, revealing that the predictions agreed well with the experimental data. This suggests that the proposed model is able to satisfactorily predict the LTC of diesel/biodiesel blends within the test range.

1. Introduction

The International Energy Agency foresees a significant increase in the world consumption of primary energy in the coming years, mainly due to the increase in the world population and the improvement of living standards (Ong et al., 2011). Moreover, regarding the energy demand of the transport sector, the vast majority of vehicles are based on fossil fuels (Kumar and Chauhan, 2013). This fact not only entails problems regarding the environment and the availability of declining reserves, but also economic and geostrategic dependence (Tong et al., 2007).

In such a scenario, a growing interest in the development and application of cleaner and more sustainable fuels has been created (Ogunkunle and Ahmed, 2019). Renewable fuels constitute a technically feasible alternative, simultaneously allowing compliance with pollutant emission standards. Among these renewable fuels, biodiesel is one of the most outstanding options for compression ignition (CI) engines (Suresh et al., 2018). Biodiesel is chemically defined as the mono-alkyl esters of long-chain fatty acids derived from vegetable oils (edible and non-edible), animal fats, waste oil or algae. The renewable origin of biodiesel minimises its life-cycle emissions of greenhouse gases. Moreover, biodiesel is considered biodegradable, environmentally friendly, non-toxic, locally available and free from sulphur and aromatic contents (Agarwal, 2007; Wei and Wang, 2021). On the other hand, the main disadvantages of biodiesel are its lower energy content and higher density and viscosity, which result in poor cold flow and spray characteristics (Rashedul et al., 2014).

Furthermore, the described context also demands significant research to find alternative technologies to meet the future international standards, especially in terms of emission of nitrogen oxides (NOx) and particulate matter (PM). However, the simultaneous reduction of NOx and PM emissions in CI engines is not easy since the formation of these pollutants presents an inverse relation: the so-called NOx-soot trade-off (Newhall, 1968; Ohigashi et al., 1971). Hence, to overcome this trade-off scenario is one capital key in current research since these emissions are

* Corresponding author.
E-mail address: joseantonio.velez@uca.es (J.A.V. Godiño).

https://doi.org/10.1016/j.egyr.2022.05.279

Nomenclature

A	Heat transfer area
B	Bore
BDC	Bottom dead center
CAD	Crank angle degree
CO	Carbon monoxide
CO_2	Carbon dioxide
Cp	Specific heat capacity
Cm	Mean piston speed
F	Fuel/air equivalence ratio
h	Instantaneous heat transfer coefficient
HC	Unburnt hydrocarbons
HRR	Heat release rate
LHV	Lower heating value
m_i	Wiebe function adjustable parameter
NHRR	Normalized heat release rate
NOx	Nitrogen oxides
p	Pressure
PM	Particulate matters
Q	Heat
R	Ideal gas constant
rpm	Revolutions per minute
t	Time
T	Temperature
TDC	Top dead center
v	Volume
v_s	Tangential speed
x_B	Fuel mass fraction burned
α_i	Wiebe function adjustable parameter
γ	Specific heat ratio
θ	Crank angle
θ_0	Wiebe function adjustable parameter
λ	Wiebe function adjustable parameter
ω	Rotational speed

strictly controlled and reduced according to new international standards (Euro VI, Tier 4). In general terms, the current methods applied to meet these stringent standards include the use of after-treatment systems, which can be costly and complex, as well as advanced combustion modes (Lilik and Boehman, 2011). Among the mentioned combustion modes, the so-called low-temperature combustion (LTC) mode stands out (Noh and No, 2017). Since NOx emissions form in the lean mixture zone when the flame temperature is over 2200 K (mainly in post flame gases) and PM is generated in rich mixture zones over 1800 K, the LTC modes basically pursue increasing the combustion pre-mixing (Yousefi et al., 2018; Shim et al., 2020). This results in the avoidance of locally rich regions, thus leading to minimisation of the peak temperatures. Therefore, LTC modes can significantly reduce both NOx and PM emissions simultaneously (Johansson, 2007) as long as performance is only minimally penalized due to an increase in brake specific fuel consumption (BSFC). Furthermore, LTC is flexible and can be applied to a wide range of fuels by choosing the proper configuration. On the other hand, carbon monoxide (CO) and unburnt hydrocarbons (HC) emissions increase as a consequence of high exhaust gas recirculation (EGR) rates and slight incomplete combustion (Jiaqiang et al., 2017). Moreover, additional drawbacks of LTC are controlling combustion phasing, extending the operating range and unacceptable noise levels (Srihari et al., 2017).

Although there are other methods, such as reactivity controlled compression ignition, gasoline compression ignition, high-efficiency clean combustion, spark-assisted compression ignition or laser-assisted compression ignition, LTC is mostly achieved through methods such as homogeneous charge compression ignition (HCCI), premixed charge compression ignition (PCCI) and partially premixed combustion (PPC) (Agarwal et al., 2017; Pachiannan et al., 2019), the latter being the mode applied in this work. In PPC mode, fuel is injected directly into the combustion chamber, close to the TDC (late direct injection) but later than in conventional CI combustion (Jacobs and Assanis, 2007; Bittle et al., 2010). Although the resulting mixture is not fully homogeneous, PPC mode leads to lower in-cylinder temperatures than PCCI, which is attractive from the NOx point of view. Apart from controlling combustion phasing better than port or early injections, late direct injection minimises wall-impingement and allows for switching to conventional CI combustion mode, since standard injectors are used (Zheng et al., 2015). In order to promote a premixed charge, which is one of the main challenges of PPC mode, long ignition delay is required (Gao et al., 2011). This is accomplished by combining different strategies, such as cooled EGR, high injection pressures and enhanced charge motion (Kawashima et al., 1998; Kimura et al., 2002). Although PPC mode results in slightly lower thermal efficiency and higher HC and soot emissions than HCCI, the former provides better control of combustion phasing. However, the combination of LTC and biodiesel allows for the reduction of CO, HC and soot emissions due to some inherent properties of biodiesel, such as its oxygen content, stoichiometric need of air and lack of aromatics (Zhu et al., 2014; Zheng et al., 2008; Saiteja and Ashok, 2021). This trend reduces the necessity of after-treatment systems, whose effectiveness is lower in LTC.

Since there is no direct actuator over autoignition, further research is currently needed to optimise sustainable LTC over wider operating ranges (Dev et al., 2017), contributing to the relevance of this study. In this line, the main aim of this work was to carry out an experimental analysis that would allow the development of a predictive tool to map biodiesel LTC under late direct injection and EGR conditions. This type of valuable tool significantly helps to achieve improved LTC, optimising EGR rates to simultaneously reduce NOx and PM emissions. Therefore, the innovative nature of this work lies in the fact that it combines two highly promising technologies in the field of sustainable internal combustion engines (biodiesel and late direct injection), also achieving objectively satisfactory results. This study was structured in three blocks. First, the details corresponding to the materials and methods applied in this work are shown, including the details corresponding to the experimental test bench, the properties of the biodiesel blends and the mathematical model used for the combustion characterisation. Next, the obtained experimental data were analysed and the proposed predictive model was developed, including the development of empirical correlations and the validation of the results. Finally, the conclusions drawn from this analysis are presented.

2. Materials and methods

2.1. Experimental setup

A four-stroke Deutz FL1 906 unit, whose technical specifications are listed in Table 1, was used to perform the experimental campaign analysed in this study. However, the original configuration of this engine was modified to work under late direct injection conditions. These modifications are required to balance the reducing emissions and the improving performance opposing effects. To attain LTC of biodiesel blends using the late direct

Table 1
Characteristics of the analysed unit.

Parameter	Value
Type	Single cylinder naturally aspirated
Ignition	Compression
Cooling system	Air-cooled
Displacement	708 cm^3
Bore	95 mm
Stroke	100 mm
Compression ratio	18.4:1
Rated power	11 kW @ 3000 rpm
Inlet valve opening	2 CAD before TDC
Inlet valve closing	36 CAD after BDC
Exhaust valve opening	36 CAD before BDC
Exhaust valve closing	2 CAD after TDC
Fuel system	Direct injection
Injection pump	Mechanical
Nozzle opening pressure	300 bar
No. of injection holes	5
Injection hole diameter	0.26 mm

Table 2
Main instrumentation specifications.

Parameter	Range	Accuracy
Crankshaft angle encoder	0°–720°	0.1°
In-cylinder pressure	0–250 bar	0.5%
Air flow	15–480 kg/h	3.0%
Fuel flow	0–30 kg/s	0.2%
Carbon monoxide	0–5000 ppm	5 ppm
Unburnt hydrocarbons	0–1000 ppm	50 ppm
Nitrogen oxides	0–1000 ppm	50 ppm

injection strategy, a series of modifications is required to enhance the mixture formation, affecting fuel evaporation and proper mixing, as follows:

- Late injection timing, with a start of injection (SOI) delayed to 10 CAD before TDC.
- Cooled EGR, typically used in CI engines (Abu-Jrai et al., 2009; Labecki and Ganippa, 2012), to reduce in-cylinder temperature and to increase the ignition delay (Pandian et al., 2010). The use of EGR is based on the introduction of a fraction of the exhaust gases in the engine cylinder, causing a decrease in the temperatures during combustion due to dilution, capacitive and chemical effects caused by combustion products (Song et al., 2021; Li et al., 2020). The disadvantages of EGR are higher emissions of CO, HC and PM (Qi et al., 2011). Particularly in late direct injection systems, the use of EGR is also related to lower thermal efficiencies.
- Internal turbulence induction mechanisms based on high-swirl chamber pistons to boost turbulence close to the TDC, promoting the evaporation of the fuel and its mixture with the air (Jaichandar and Annamalai, 2021; Saito et al., 1986). Therefore, the original piston was replaced by a new one with a ratio between cylinder and chamber diameters of 2.8.
- Maximum injection pressure was increased to 650 bar from the original 450 bar. This modification implies a reduction in the injection duration and an increase in the surface-volume ratio of the fuel droplets, which positively contribute to mixture formation (Hountalas et al., 2003).

The test bench scheme is shown in Fig. 1. The rotational speed was controlled with a 25 kW electric dynamometric brake. The main specifications of the relevant instrumentation, connected to a data acquisition system (1 MHz, 16 bit), is characterised in Table 2 (Godiño et al., 2022):

2.2. Fuel and operating conditions

The tests involved in this work were carried out using blends of EN-590 diesel fuel and EN-14214 biodiesel. Biodiesel from rapeseed (*Brassica napus*), pertaining to the mustard family, was specifically used in this study. A typical fatty acid methyl ester (FAME) composition of rapeseed biodiesel mainly includes 65% oleate (C18:1), 20% linoleate (C18:2), 7% linolenate (C18:3) and, finally, 5% palmitate (C16:0) (Kumar and Chauhan, 2013), where the first figure represents carbon atoms and the second refers to double bonds. The physical and chemical properties of biodiesel are conditioned by the FAME composition (Kumar and Chauhan, 2013; Ashraful et al., 2014), which affects engine performance and emissions. Three fuel blends were considered in this work, which are defined by their biodiesel volume ratio: 0% (B0), 30% (B30) and, finally, 65% (B65). The properties of the different fuel blends, which were characterised in the laboratory, are shown in Table 3.

Each fuel blend was analysed under different operating conditions, as shown in Table 4. Furthermore, the control of the external EGR was 'constant fuelling rate', which led to equivalence ratio increasing with the EGR rate although the injected fuel remains constant.

2.3. Mathematical modelling

2.3.1. Experimental HHR

The most common method for combustion characterisation is use of the heat release rate (HRR), which allows for observations that are not apparent from in-cylinder pressure. HRR curves were obtained from the chamber pressure data using a zero-dimensional model (perfect mixing reactor with time-dependent chemical composition) (Heywood, 2018). Although current CFD models provide detailed results, they involve intensive computational resources, hence zero-dimensional models are used for fast preliminary analysis of engines.

Moreover, CFD models depend heavily on the initial and boundary conditions imposed for simulation. Additionally, the in-cylinder pressure trace derived from these simplified models constitutes a very useful tool for studying the effect of different operating parameters on the main pollutant emission.

The combination of the state equation of ideal gases and the first principle of thermodynamics allows the characterisation of the experimental HRR curves, as follows (Foster, 1985):

$$HRR = \frac{1}{\gamma - 1}\left(p \cdot \gamma \cdot \frac{dv}{d\theta} + v \cdot \frac{dp}{d\theta}\right) - \frac{p \cdot v}{(\gamma - 1)^2} \cdot \frac{d\gamma}{d\theta} - \frac{dQ_{LOSS}}{d\theta} \quad (1)$$

The properties of the different chemical components were considered variable with chamber temperature (Eq. (2)) (Depcik et al., 2007):

$$\frac{C_P}{R} = c_1 + c_2 \cdot T + c_3 \cdot T^2 + c_4 \cdot T^3 + c_5 \cdot T^4 \quad (2)$$

The heat losses through the cylinder walls ($^{dQ_{LOSS}}/_{d\theta}$) were characterised using Eq. (3), involving a heat transfer coefficient (h), the exposed cylinder surface (A), the temperature difference between the gas and the wall ($T - T_{wall}$) and, finally, the engine rotational speed (ω). Moreover, an instantaneous cylinder average heat transfer coefficient (Eq. (4)) was considered (Woschni, 1967), with parameters K_1 and K_2 defined in Table 5.

$$\frac{dQ_{LOSS}}{d\theta} = \frac{dQ_{LOSS}}{dt} \cdot \frac{dt}{d\theta} = h \cdot A \cdot (T - T_{wall}) \cdot \frac{1}{\omega} \quad (3)$$

$$h = 3.26 \cdot \frac{p^{0.8}}{B^{0.2} \cdot T^{0.55}} \cdot \left[K_1 \cdot c_m + K_2 \cdot \frac{V_d \cdot T_{ivc}}{p_{ivc} \cdot v_{ivc}} \cdot (p - p_m)\right]^{0.8} \quad (4)$$

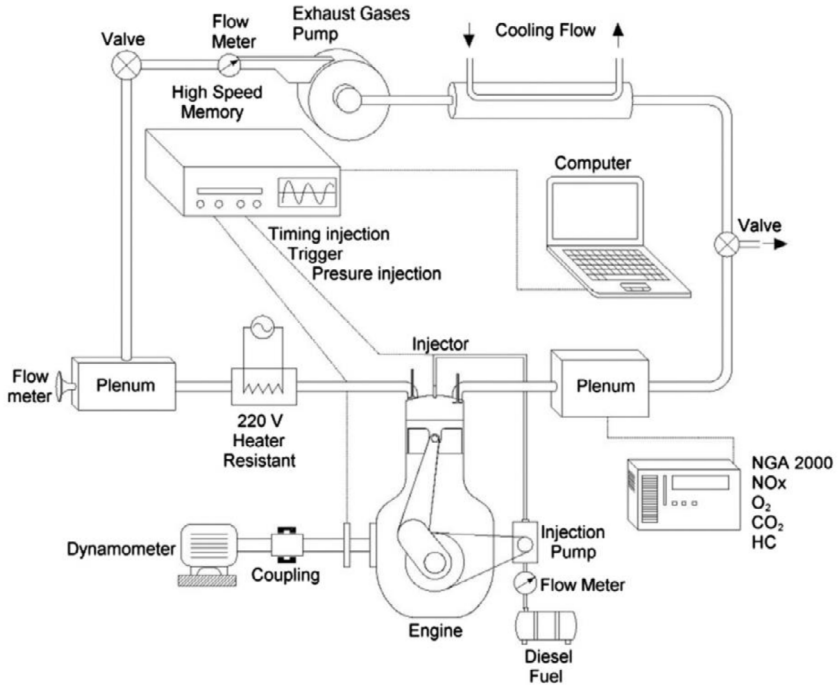

Fig. 1. Schematic diagram of the engine setup.

Table 3
Properties of the fuel blends.

Fuel blend	Density @ 15 °C (kg/m^3)	Viscosity @ 40 °C (cSt)	LHV (MJ/kg)	95% distillation temperature (°C)	Cetane index
B0	832.0	2.9	43.1	175–350	47.0
B30	858.8	3.3	42.2	200–390	47.6
B65	865.5	4.0	41.2	207–405	52.2

Table 4
Tested operating conditions.

Parameter	Value
Speed (rpm)	1800
	2100
	2400
Fuel/air equivalence ratio (–)	0.20
	0.30
	0.45
	0.60
EGR (%)	From 0%
	Up to misfiring condition (max. 41%)
Fuel blend (–)	B0
	B30
	B65

Table 5
K_1 and K_2 used heat losses model (Eq. (4)).

	Compression	Combustion and expansion
K_1	$2.28 + 0.308 \cdot \frac{v_s}{c_m}$	$2.28 + 0.308 \cdot \frac{v_s}{c_m}$
K_2	0	$3.24 \cdot 10^{-3}$

The effect on transfer coefficient caused by turbulence mechanisms was modelled through the mixture tangential speed (v_s) (Jiménez-Espadafor et al., 2009). Finally, it should be noted that, for each test considered, the chamber pressure curve used in the analysis results from averaging 150 consecutive cycles (COVIMEP<5%) (Heywood, 2018; Rakopoulos et al., 2017)

2.3.2. Predicted HRR

In order to develop the proposed predictive model this work was based on continuous functions. These empirical functions represent a computationally effective and fast method to predict the fuel burn rate, which is used as an input into more complex numerical models to assist engines analysis. This engineering approach, initially proposed by Ivan Wiebe (Ramos, 1989), was conceptually based on the combustion reaction kinetics, but bypassing the chemical details and resulting in an empirical heat release law. Initially, a standard single-Wiebe law, as a function of the crankshaft position θ, was used, as follows (Eq. (5)):

$$x_B = 1 - exp\left[-\left(\frac{\theta - \theta_0}{\alpha}\right)^{m+1}\right] \quad (5)$$

where x_B is the fuel mass fraction burned, θ_0 is the start of combustion, α is proportional to the combustion duration and, finally, m is the shape factor (Yeliana et al., 2011). The parameters in the single-Wiebe law were computed using the least-squares fit method, resulting in three parameters to be adjusted (θ_0, α, m) for each specific operating condition (Section 2.2). However, as demonstrated in Section 3.2, the single-Wiebe law was not able to reproduce the experimental heat release rate associated to the LTC of diesel/biodiesel blends characterised in this work. Hence, the measured heat release rate consists of two phases: a premixed stage (the so-called "mode 1"), controlled by the oxidation rate, and a diffusive stage (the so-called "mode 2"), controlled by the mixing process (Ghojel et al., 2006). As previously researchers such as Pugachov, Ghojel, Watson and Miyamoto did in different

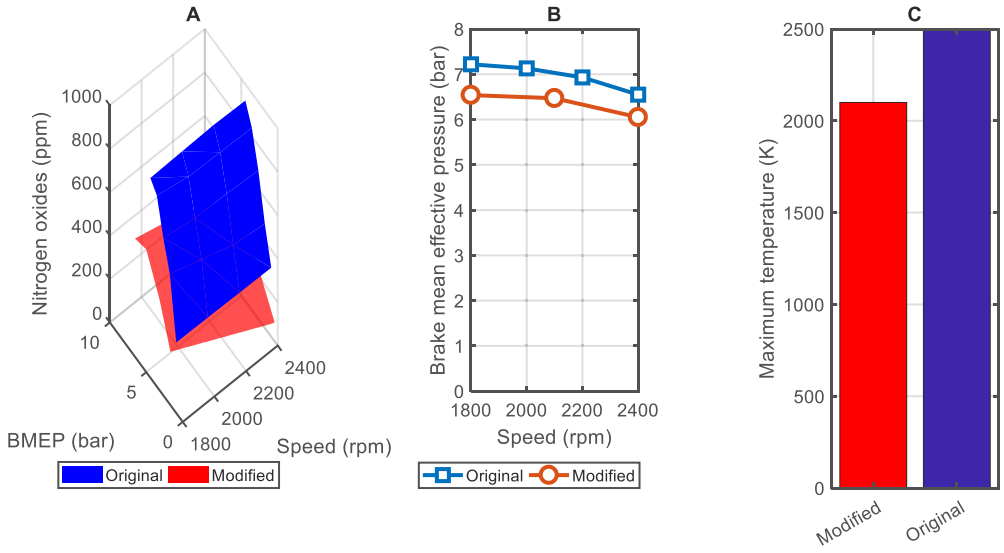

Fig. 2. NOx emissions (A), brake mean effective pressure (B) and maximum average temperature (C) (0% EGR).

applications (Ghojel, 2010), a double-Wiebe function involving six adjustable parameters (λ, θ_0, α_1, m_1, α_2, m_2) was proposed (Eq. (6)) to reproduce the experimental burn rate:

$$x_B = \lambda \left\{1 - exp\left[-\left(\frac{\theta - \theta_0}{\alpha_1}\right)^{m_1+1}\right]\right\} + (1-\lambda)\left\{1 - exp\left[-\left(\frac{\theta - \theta_0}{\alpha_2}\right)^{m_2+1}\right]\right\} \quad (6)$$

This type of double-Wiebe functions were successfully used in the past to model the heat release process in diesel LTC applications (Yasar et al., 2008; Glewen et al., 2009).

3. Results and discussion

3.1. Experimental analysis

The demonstration of the attainment of LTC is not feasible using conventional diagnosis instrumentation (Bittle et al., 2010). LTC attainment is often justified if the injection pulse is shorter than the ignition delay. However, this situation does happen at low load in many conventional CI engines, not meaning LTC attainment. Additionally, it is not accurate to state that injection is completed before the start of combustion since chemical mechanisms always start before the end of injection. Hence, to justify the attainment of biodiesel LTC in this work the most practical tool is to stablish a comparison between some key results of the original and the modified configurations (Fig. 2). In addition to the inherent sustainability derived from the use of biodiesel, the adopted modifications led to a 50% reduction in NOx emissions at high load (Fig. 2A). Additionally, the engine modification did not result in a significant reduction of performance, since the peak value of brake mean effective pressure (BMEP) showed a shortfall lower than 7% at 2400 rpm (Fig. 2B). This drastic reduction in NOx emissions while practically maintaining the original performance levels justified the attainment of a sustainable LTC in this work. As already mentioned in Section 1, this performance improvement is possible due to the reduction of the average combustion temperature, quantified by 16% in this particular case (from 2500 K in the conventional CI mode to 2100 K in the modified configuration, Fig. 2C). This figure is in line with the 15% decrease proposed by Pachiannan et al. (2019).

To provide better understanding, the effect of biodiesel percentage over LTC main features was analysed. Fig. 3 illustrates the results derived from the methodology described in Section 2.3.1, comparing in-cylinder pressure, normalised HRR traces ($NHRR = {}^{dx_B}/_{d\theta}$) and average temperature for different fuel blends. As derived from experimental HRR curves, two different phases compose the combustion: a more vigorous premixed phase and a less intense diffusive phase. This allows for the conclusion that although the previous results suggest LTC attainment, the fuel/air mixture is not fully homogeneous, as expected for PPC mode. Regarding HRR, Fig. 3 shows shorter ignition delays when higher fractions of biodiesel are tested. This is a result of the different cetane number of each fuel blend, which is higher for biodiesel. On the other hand, the lower the biodiesel fraction the higher the maximum pressure, pressure rise rate and HRR peaks, which is attributed to the longer evaporation and mixing period before the start of combustion. The in-cylinder temperature traces shown in Fig. 3(C) reveals a general decrease in comparison to the conventional CI combustion, as mentioned in previous paragraphs.

Fig. 4 shows ignition delay (A), combustion duration (B) and brake efficiency (C) as a function of brake mean effective pressure. Ignition delay is the period (or angle) between the start of injection and the start of combustion (SOC). The SOC is typically established as $X_B^{SOC} = 5\%$ to avoid the noise in the experimental signal (Liu and Dumitrescu, 2019). Similarly, combustion duration is defined as the interval between the SOC and end of combustion (EOC). Since the final phase of combustion is slow and without actual attractiveness, the EOC is typically established as $X_B^{EOC} = 95\%$ (Sun et al., 2017). It is observed that the ignition delay is reduced as a consequence of the heating effect derived from the load increase. Moreover, the ignition delay increases because of the lower cetane number when the biodiesel fraction in the blend is reduced. Fig. 4 also shows that combustion duration is proportional to BMEP, as a consequence of the longer time required for the oxidation of higher amounts of fuel. Additionally, it is observed that the higher biodiesel fraction in the blend the shorter the combustion duration. This trend is related to the higher mixture temperature derived from shorter delays. Additionally, oxygenated fuels produce more reactive radicals, which also contributes to shorter combustion duration. Furthermore, Fig. 4 illustrates an inverse relationship between ignition delay and combustion duration. Hence, the longer the delay the shorter the duration, as a consequence of the additional time

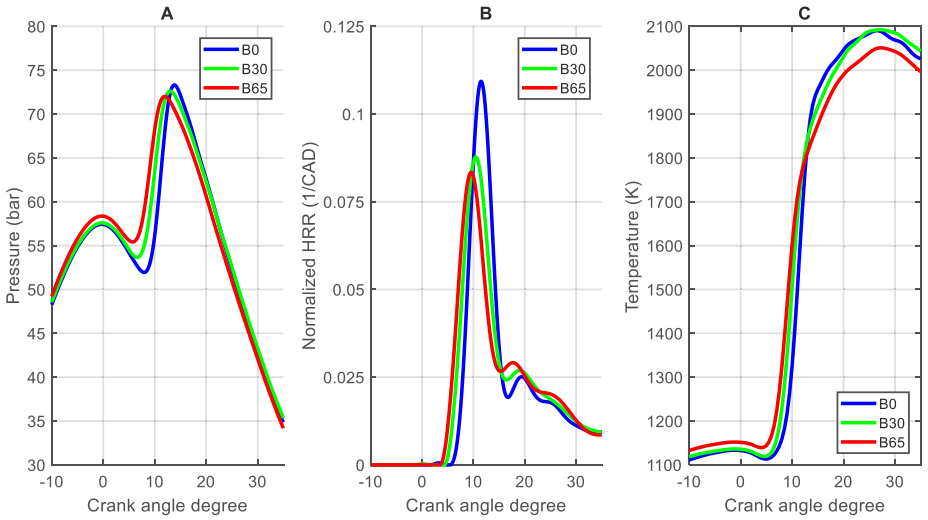

Fig. 3. Chamber pressure (A), normalised heat release rate (B) and average temperature (C) (2100 rpm, F = 0.45, 0% EGR).

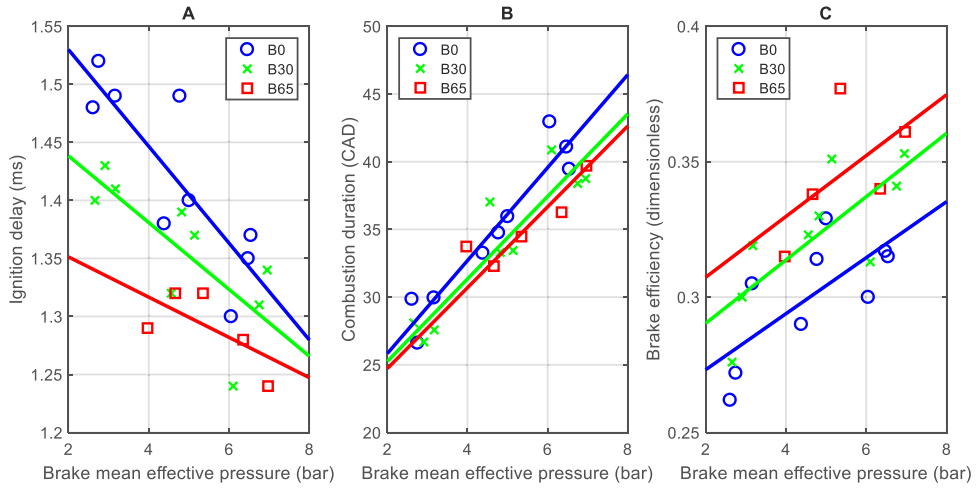

Fig. 4. Ignition delay (A), combustion duration (B) and brake efficiency (C) (0% EGR).

for fuel evaporation and mixing. This results in a faster burn rate in the premixed phase and, finally, in lower combustion duration. However, longer delays move combustion further in the expansion stroke, where temperatures are lower. Additionally, over-mixing may result in regions that are too lean to burn. Both charge quenching and over-mixing result in higher products of incomplete combustion (Han et al., 2009). Finally, Fig. 4 also reveals that the higher biodiesel fraction in the blend the higher the brake efficiency, since the combustion takes place closer to the TDC (refer also to Fig. 3), increasing the expansion work. This trend derives from the lower values of both the ignition delay and the combustion duration, as previously discussed. On the contrary, longer ignition delays penalize brake efficiency due to incomplete combustion.

Regarding the pollutant emission, Fig. 5 shows the data corresponding to CO, HC, soot (characterised from the smoke opacity index) and NOx as a function of brake mean effective pressure. The higher proportion of biodiesel the lower the emissions of CO, HC and soot, as demonstrated in Fig. 5 (subplots A, B and C respectively). This reduction of emissions derives from some characteristic properties of biodiesel, such as its oxygen content, lower stoichiometric need of air and lack of aromatics. Additionally, incomplete combustion is reduced due to the aforementioned shorter ignition delay corresponding to biodiesel. Contrarily, an increase of biodiesel percentage results in slightly higher NOx emissions (Fig. 5 subplot D). Apart from the already mentioned increase in the combustion temperature (higher cetane number), this increase is also associated to a set of different effects, as follows:

- Biodiesel has a higher speed of sound and isentropic bulk modulus of compressibility than fossil diesel, which results in an advance in fuel injection timing.
- Biodiesel has a higher adiabatic flame temperature due to the presence of unsaturated molecules in its composition. Additionally, faster combustion processes increase the in-cylinder temperature and residence time.
- The different properties of biodiesel regarding mixture formation influence the portion of energy released in the premixed and diffusive stages.

3.2. HRR curve fitting

After discussing the experimental analysis carried out, the development of the proposed predictive model is described, starting with the curve fitting procedure. Fig. 6 shows two comparisons between the experimental and the modelled HRR curves. Both

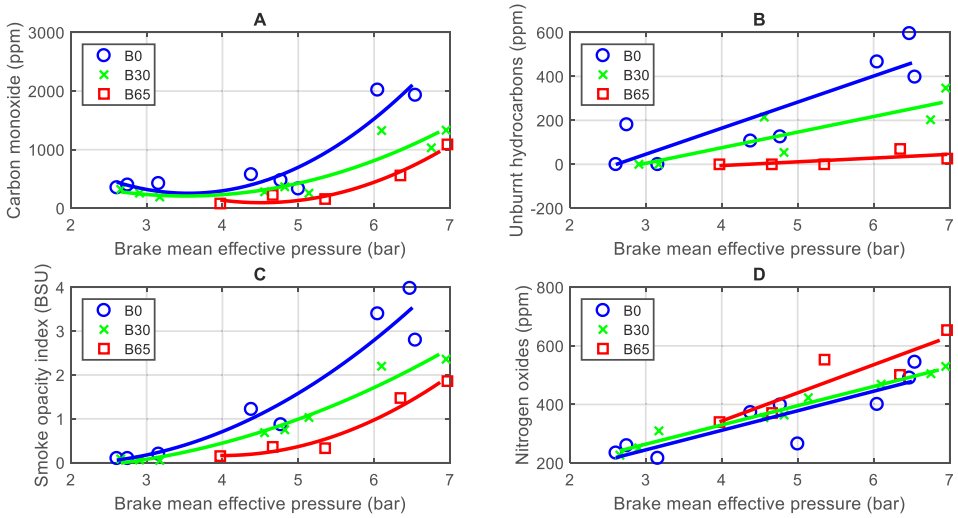

Fig. 5. Carbon monoxide (A), unburnt hydrocarbons (B), smoke opacity index (C) and nitrogen oxides (D) emissions (0% EGR).

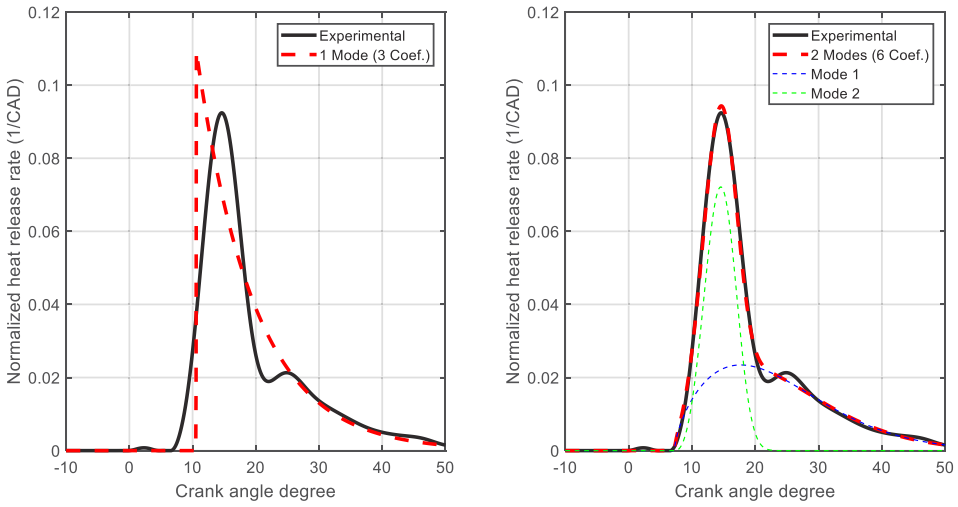

Fig. 6. Experimental and modelled normalised heat release rate (B30, 2400 rpm, F = 0.3, 11% EGR). Left: Single-Wiebe law (3 coefficients). Right: Double-Wiebe law (6 coefficients).

comparisons correspond to the same operating conditions. Specifically, the left plot of Fig. 6 compares the experimental trace with the curve derived from the single-Wiebe law. A preliminary conclusion can be drawn that single-Wiebe function fails to model the HRR in late direct injection LTC. However, the right plot of Fig. 6 demonstrates that the double-Wiebe law accurately matches the experimental HRR trace. The high level of accuracy of the resulting prediction, without this entailing a significant increase in computational cost, is noteworthy. Furthermore, Fig. 6 (right side) depicts the two summands that make up the employed Wiebe law, namely "Mode 1" and "Mode 2".

Although Fig. 6 clearly shows the need for the double-Wiebe function, the box plot analysis corresponding to the six fitted parameters (Fig. 7) revealed the existence of an excessive number of outliers. This would be highly detrimental in the later phase of defining correlations for the prediction of the Wiebe parameters, being necessary to modify the proposed approach. Since the interquartile ranges ($Q_3 - Q_1$) corresponding to parameters m_1 and especially m_2 are comparatively smaller than in the rest of the Wiebe parameters (meaning low dispersion), fixing the values of m_1 and m_2 is proposed. Consequently, both parameters will be independent from the operating conditions, with each one adopting the value corresponding to its median ($m_1 = 0.50$ and $m_2 = 2.25$). This approach results in a modified double-Wiebe law (Eq. (7)), which involves four adjustable parameters (λ, θ_0, α_1, α_2):

$$x_B = \lambda \left\{ 1 - exp\left[-\left(\frac{\theta - \theta_0}{\alpha_1} \right)^{0.50+1} \right] \right\} + (1-\lambda) \left\{ 1 - exp\left[-\left(\frac{\theta - \theta_0}{\alpha_2} \right)^{2.25+1} \right] \right\} \quad (7)$$

After modifying the approach of the Wiebe function, the least squares fit method was repeated to adjust the four parameters involved in Eq. (7). Fig. 8 illustrates the comparison between the experimental HRR and the trace derived from the modified double-Wiebe function for the same operating condition in Fig. 6. This figure allows for the conclusion that although the adjustability of the four-coefficient function is logically lower than that of a six-coefficient law, the proposed modified double-Wiebe law is perfectly valid to reproduce the development of the late direct injection LTC analysed in this work. Additionally, as will be detailed in Section 3.3, the modified approach has allowed the practical elimination of outliers, which will make

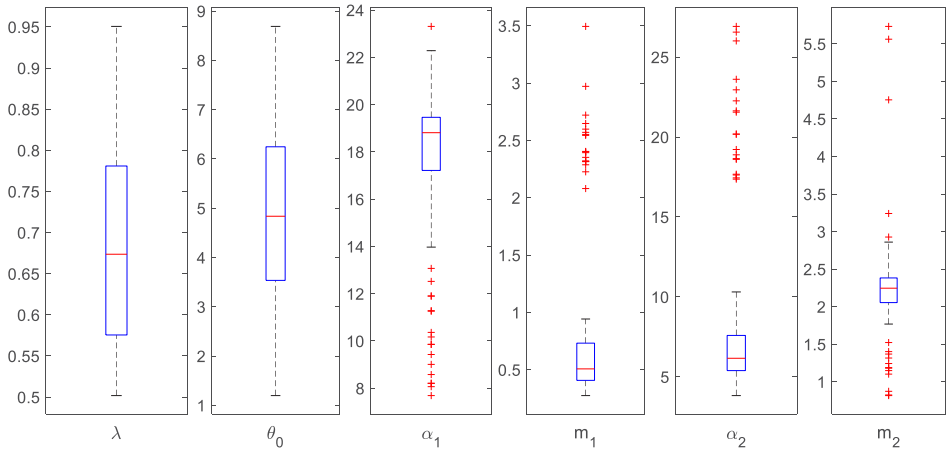

Fig. 7. Box plot of six fitted parameters of the double-Wiebe law.

possible the development of more precise correlations for the Wiebe parameters.

3.3. Wiebe parameter correlations

Once the four adjustable parameters corresponding to the modified double-Wiebe law were accurately fitted, a multiple regression methodology was used in order to correlate the Wiebe parameters with the operating conditions. Consequently, HRR and in-cylinder pressure curves could be predicted within the tested operating range, constituting a powerful design tool. Hence, the four adjustable parameters were expressed as mathematical functions of the operating variables considered in this work. The inherent limitations derived from the use of empirical laws was balanced by the development of an extensive experimental analysis. However, before fitting the coefficients of the correlations, a multifactorial variance analysis was performed in order to determine the operating variables that have a statistically significant effect on each Wiebe parameter. The results of this analysis, whose box plot is depicted in Fig. 9, show that all of the four operating variables analysed (percentage of biodiesel, speed, fuel/air equivalence ratio and percentage of external EGR) are statistically significant in relation to the four Wiebe parameters. Additionally, the existence of only one outlier in Fig. 9, as a consequence of the modified approach proposed in Section 3.2, is noteworthy.

Specifically, the use of polynomial correlations was proposed, which have allowed for satisfactory results in similar applications (Maroteaux and Saad, 2013). Despite their simplicity, polynomial correlations present a great potential in predicting HRR parameters due to the low computational effort. The validity of such a predictive approach is limited to the operating conditions used for determining the model parameters, which are defined in Section 2.2. The functions that will be used to develop Wiebe parameters correlations will be a cubic polynomial without interactions (Eq. (8)), thus limiting the potential appearance of the Runge phenomenon, consisting of significant numerical oscillations for points located outside the calibration range of the correlation produced by higher order terms (Sun et al., 2017). This decision implies the adjustment of 13 coefficients for each Wiebe parameter, which were determined by applying a least squares fitting procedure (Table 6). The goodness of the results obtained through this method is captured by the correlation coefficients and is shown in Fig. 10, validating the modified approach proposed in the previous section to enhance the predictability of the Wiebe parameters.

$$X = \beta_0 + \sum_{i=1}^{3} \beta_i^{BIO} \cdot \left(\frac{\%BIO}{100}\right)^i + \sum_{i=1}^{3} \beta_i^{RPM} \cdot \left(\frac{RPM}{10000}\right)^i$$

Table 6
Correlation coefficients for the adjustable parameters of the modified double-Wiebe law.

	λ	θ_0	α_1	α_2
β_0	1.006E0	−1.534E1	3.007E1	1.471E1
β_1^{BIO}	3.552 E0	3.568E1	2.331E2	1.053E2
β_2^{BIO}	−1.582E1	−1.669E2	−1.113E3	−4.968E2
β_3^{BIO}	1.615E1	1.742E2	1.161E3	5.178E2
β_1^{RPM}	1.055E1	−9.903E−1	−1.667E2	6.102E1
β_2^{RPM}	−2.673E1	−1.259E1	3.124E2	1.114E2
β_3^{RPM}	1.952E1	−2.698E1	6.019E2	−5.105E2
β_1^{F}	−3.893E−1	−5.475E−1	4.359E1	−3.520E1
β_2^{F}	1.266E0	−2.910E−2	−3.992E1	6.837E1
β_3^{F}	−5.315E−1	−2.445E0	1.139E1	−3.858E1
β_1^{EGR}	5.000E−3	−5.822E−1	1.119E0	5.153E−1
β_2^{EGR}	2.213E−1	−9.393E−1	1.399E1	1.988E1
β_3^{EGR}	4.710E−2	5.421E−1	−3.111E1	−2.143E1
R^2	0.959	0.998	0.957	0.909

$$+ \sum_{i=1}^{3} \beta_i^{F} \cdot F^i + \sum_{i=1}^{3} \beta_i^{EGR} \cdot \left(\frac{\%EGR}{100}\right)^i \quad (8)$$

3.4. Model validation

To determine the validity of the developed model, the previous correlations were used to obtain estimated HRR curves and this information was used to reconstruct in-cylinder pressure traces by inverting the methodology stated in Section 2.3.1. In Figs. 11 and 12, the modelled HRR and pressure traces are compared to the experimental curves for different fuel blends and different percentages of external EGR, respectively. These figures show that the proposed predictive model gives very reliable results compared to experimental measurements since modelled and experimental traces are practically coincident. The model accuracy is remarkable in terms of SOC and maximum pressure, regarding both magnitude and CAD. Specifically, the average maximum relative error in pressure trace, generally located close to SOC, is 4.15%, while the average absolute deviation of the maximum pressure is 0.29 bar (typically overpredicted).

The BMEP is an additional indicator to test the accuracy of the predictive model within the tested range. Effective parameters were obtained from the integration of modelled in-cylinder pressure and applying an ad hoc mechanical losses model as

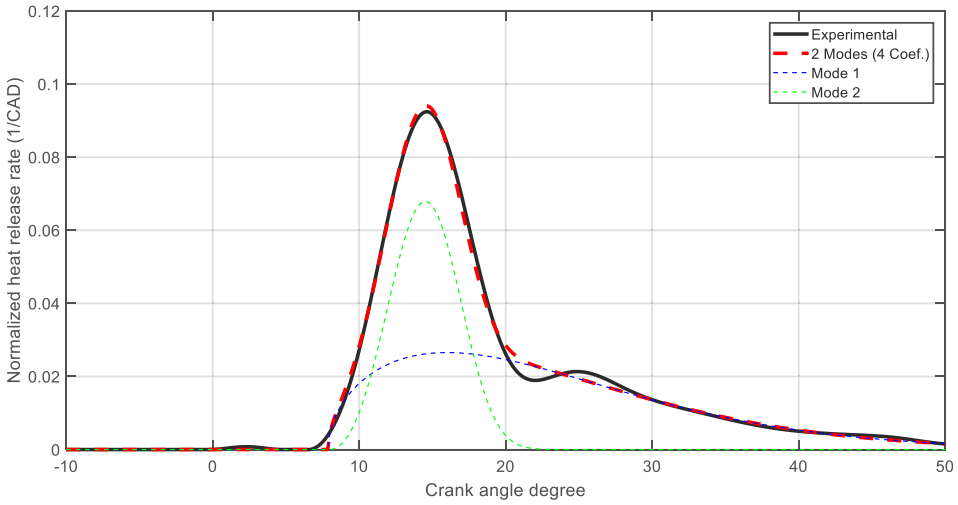

Fig. 8. Experimental and modelled normalised heat release rate using a modified double-Wiebe law (4 coefficients), (B30, 2400 rpm, F = 0.3, 11% EGR).

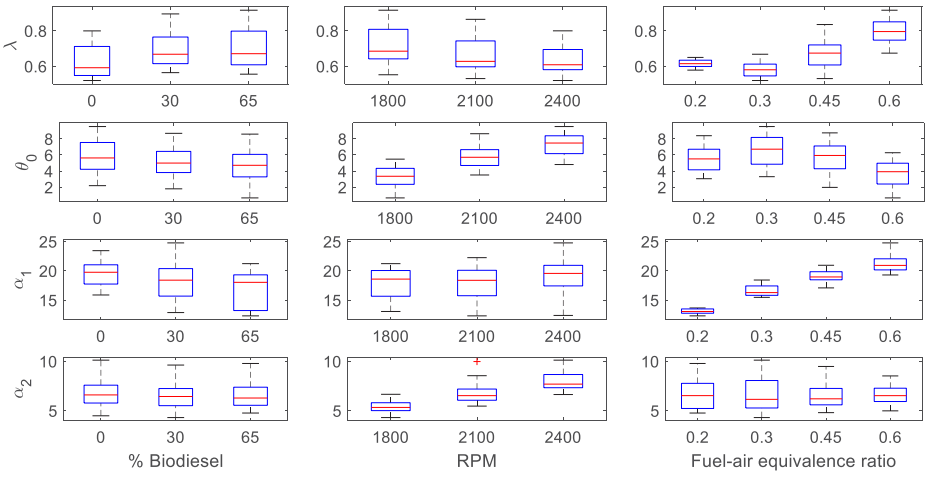

Fig. 9. Box plot of the four adjustable parameters corresponding to the modified double-Wiebe law.

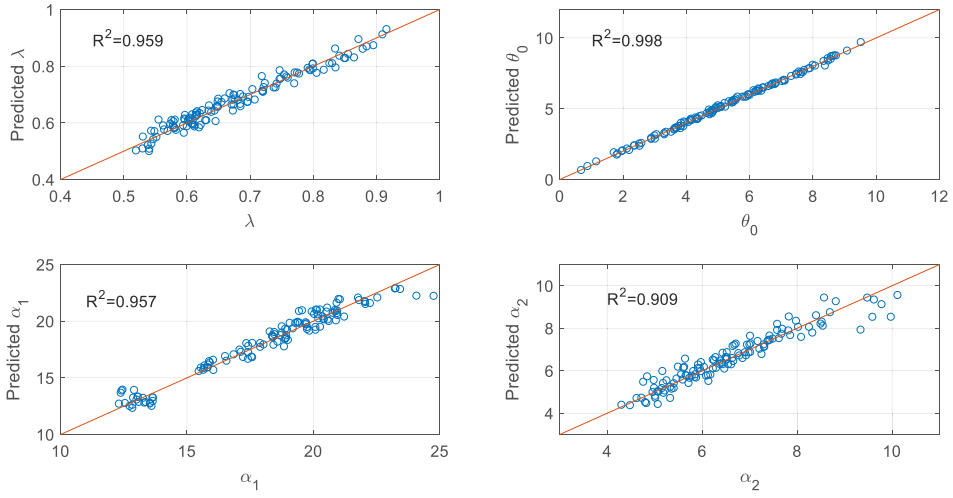

Fig. 10. Adjusted and predicted parameters corresponding to the modified double-Wiebe law.

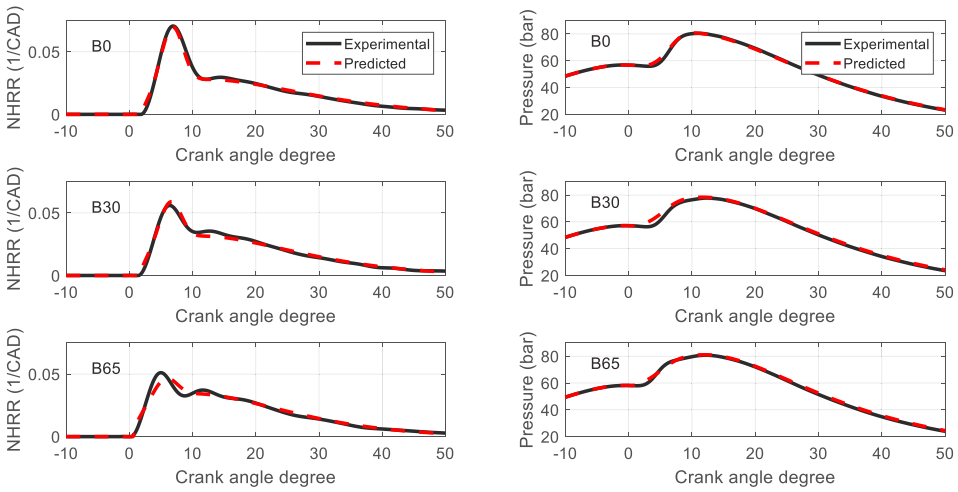

Fig. 11. Normalised heat release rate (left) and in-cylinder pressure (right) (1800 rpm, F = 0.6, 0% EGR).

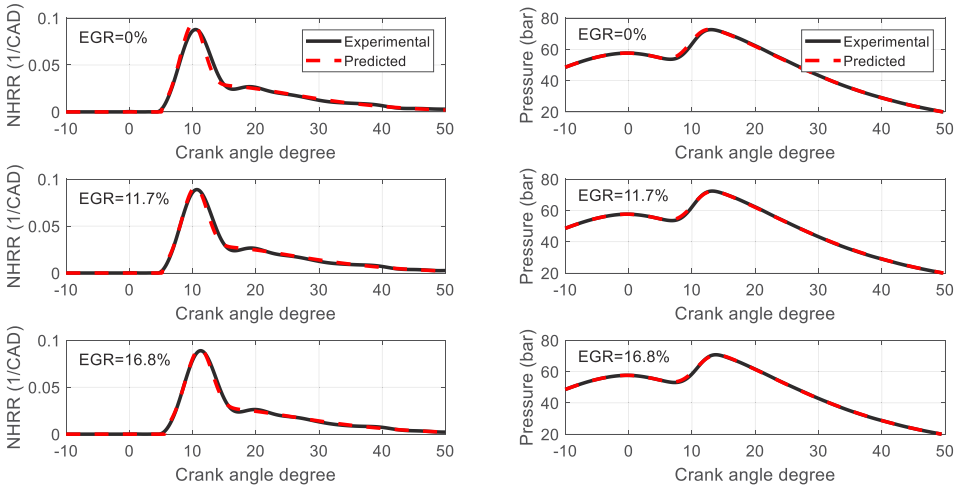

Fig. 12. Normalised heat release rate (left) and in-cylinder pressure (right) (B30, 2100 rpm, F = 0.45).

a function of engine rotational speed (Heywood, 2018). Fig. 13 shows the good agreement between experimental and modelled BMEP. Despite the mentioned general agreement (R^2 = 0.988), the largest deviations are located at high loads, where some overpredicted values are identified.

4. Conclusions

In the present study, an experimental analysis was carried out to assess both thermal performance and emissions and to propose a predictive tool aiming to characterise the innovative LTC of diesel/biodiesel blends with late direct injection (PPC mode). In order to provide the predictive model with enough prediction capability, an extensive set of operating variables (Section 2.2) involving different conditions of percent biodiesel in fuel blend, rotational speed, fuel/air equivalence ratio and percent external EGR was experimentally tested to fit the proposed empirical laws.

The developed experimental analysis confirmed the ability of LTC to reduce NOx emissions (50% reduction), maintaining thermal performance, compared to conventional diesel configuration. Additionally, this study proved the significant reduction in the emissions of CO, HC and soot associated to biodiesel compared to fossil diesel (more than 66% decrease for B65 at high load), due some characteristic properties of biodiesel, such as its oxygen content, lower stoichiometric need of air and lack of aromatics. However, these properties of biodiesel also led to higher NOx emissions compared to fossil diesel (20% increase for B65 at high load).

After analysing other alternatives, the optimal solution in terms of predictability consisted in the experimental HRR to be fitted to a modified double-Wiebe function involving four adjustable parameters (λ, θ_0, α_1, α_2). Then, predictive correlations between Wiebe parameters and operating conditions were obtained, resulting in correlation coefficients ranging from 0.909 to 0.998. The validation of the predictive model, focused on pressure trace, revealed that the predictions agreed well with the experimental data, which suggests that the proposed model is capable of reasonably predicting the LTC mode in the range addressed in the present work. Specifically, the average maximum relative error was 4.15% and the average absolute deviation of the maximum pressure was 0.29 bar. Additionally, the goodness of the proposed model was validated by comparing values of measured and predicted BMEP (R^2 = 0.988). This accuracy would make it possible to study the effect of different operating parameters on the main pollutant emission from models based on the in-cylinder pressure trace.

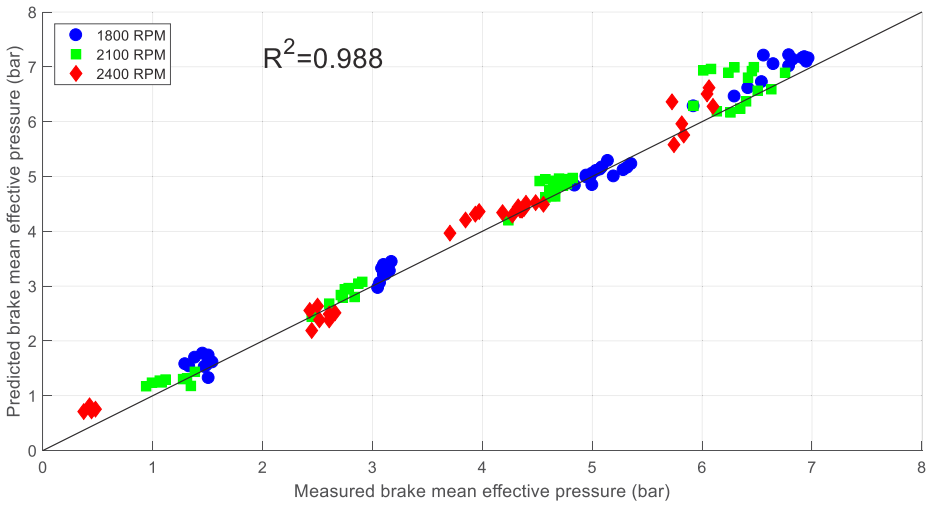

Fig. 13. Measured and predicted brake mean effective pressure.

Considering the previous results, this predictive model is considered a relevant tool that may significantly help to optimise sustainable biodiesel LTC. Moreover, in order to extent the limited operating range of biodiesel LTC mode, these predictive models could help in the assessment of the combination of LTC with advanced hybrid powertrains. Differently from time-consuming CFD codes, this predictive model is also suitable for implementation of Hardware in the Loop (HiL) simulations used in engine control, being run in real-time applications due to its computational simplicity.

CRediT authorship contribution statement

José Antonio Vélez Godiño: Formal analysis, Validation, Investigation, Writing – original draft. **Miguel Torres García:** Visualization, Data curation. **Francisco José Jiménez-Espadafor Aguilar:** Conceptualization, Methodology, Supervision.

Declaration of competing interest

The authors declare that they have no known competing financial interests or personal relationships that could have appeared to influence the work reported in this paper.

Acknowledgements

The authors would like to acknowledge the Council for Economy of the Regional Government of Andalusia (Spain) and the University of Cádiz (UCA Own Plan to Support and Stimulate Research and Transfer) for their financial support under AT17-5934-US and PB2022-041, respectively.

References

Abu-Jrai, A., et al., 2009. Performance, combustion and emissions of a diesel engine operated with reformed egr. Comparison of diesel and GTL fuelling. Fuel 88 (6), 1031–1041.
Agarwal, Avinash Kumar, 2007. Biofuels (alcohols and biodiesel) applications as fuels for internal combustion engines. Prog. Energy Combust. Sci. 33 (3), 233–271.
Agarwal, Avinash Kumar, Singh, Akhilendra Pratap, Maurya, Rakesh Kumar, 2017. Evolution, challenges and path forward for low temperature combustion engines. Prog. Energy Combust. Sci. 61, 1–56.
Ashraful, A. Masjuki, et al., 2014. Production and comparison of fuel properties, engine performance, and emission characteristics of biodiesel from various non-edible vegetable oils: a review. Energy Convers. Manage. 80, 202–228.
Bittle, J.A., Knight, B.M., Jacobs, T.J., 2010. Investigation into the use of ignition delay as an indicator of low-temperature diesel combustion attainment. Combust. Sci. Technol. 183 (2), 138–153.
Depcik, Christopher, et al., 2007. Instructional use of a single-zone, premixed charge, spark-ignition engine heat release simulation. Int. J. Mech. Eng. Educ. 35 (1), 1–31.
Dev, S., Chaudhary, H.B., Gothekar, S., Juttu, S., Walke, N.H., Marathe, N.V., 2017. Advanced Low Temperature Combustion Approach for BS VI. SAE Technical Paper; 2017-26-0042.
Foster, David E., 1985. An overview of zero-dimensional thermodynamic models for IC engine data analysis. SAE Trans. 436–449.
Gao, Zhiming, et al., 2011. Using a phenomenological computer model to investigate advanced combustion trajectories in a CIDI engine. Fuel 90 (5), 1907–1918.
Ghojel, J.I., 2010. Review of the development and applications of the wiebe function: a tribute to the contribution of ivan wiebe to engine research. Int. J. Engine Res. 11 (4), 297–312.
Ghojel, Jamil, Honnery, Damon, Al-Khaleefi, Khaled, 2006. Performance, emissions and heat release characteristics of direct injection diesel engine operating on diesel oil emulsion. Appl. Therm. Eng. 26 (17–18), 2132–2141.
Glewen, William J., et al., 2009. Analysis of cyclic variability in spark-assisted HCCI combustion using a double wiebe function. Proc. Combust. Inst. 32 (2), 2885–2892.
Godiño, José Antonio Vélez, García, Miguel Torres, Jiménez-Espadafor Aguilar, Francisco José, 2022. Experimental analysis of late direct injection combustion mode in a compression-ignition engine fuelled with biodiesel/diesel blends. Energy 239, 121895.
Han, Manbae, Assanis, Dennis N., Bohac, Stanislav V., 2009. Sources of hydrocarbon emissions from low-temperature premixed compression ignition combustion from a common rail direct injection diesel engine. Combust. Sci. Technol. 181 (3), 496–517.
Heywood, John B., 2018. Internal Combustion Engine Fundamentals. McGraw-Hill Education.
Hountalas, D.T., et al., 2003. Effect of Injection Pressure on the Performance and Exhaust Emissions of a Heavy Duty DI Diesel Engine. No. 2003-01-0340. SAE Technical Paper.
Jacobs, Timothy J., Assanis, Dennis N., 2007. The attainment of premixed compression ignition low-temperature combustion in a compression ignition direct injection engine. Proc. Combust. Inst. 31 (2), 2913–2920.
Jaichandar, S., Annamalai, K., 2021. Effects of open combustion chamber geometries on the performance of pongamia biodiesel in a DI diesel engine. Fuel 98, 272–279.
Jiaqiang, E., et al., 2017. Effect of different technologies on combustion and emissions of the diesel engine fueled with biodiesel: a review. Renew. Sustain. Energy Rev. 80, 620–647.
Jiménez-Espadafor, F.J., Garcia, M.T., Herrero, J.A.C., Villanueva, J.A.B., 2009. Effect of turbulence and external exhaust gas recirculation on HCCI combustion mode and exhaust emissions. Energy Fuels 23 (9), 4295–4303.
Johansson, Bengt, 2007. Homogeneous charge compression ignition: the future of IC engines? Int. J. Veh. Des. 44 (1–2), 1–19.
Kawashima, Jun-ichi, Ogawa, Hiroshi, Tsuru, Yoshiyuki, 1998. Research on a variable swirl intake port for 4-valve high-speed DI diesel engines. SAE Trans. 2212–2229.
Kimura, Shuji, et al., 2002. An experimental analysis of low-temperature and premixed combustion for simultaneous reduction of NOx and particulate emissions in direct injection diesel engines. Int. J. Engine Res. 3 (4), 249–259.

Kumar, Niraj, Chauhan, Sant Ram, 2013. Performance and emission characteristics of biodiesel from different origins: a review. Renew. Sustain. Energy Rev. 21, 633–658.
Labecki, L., Ganippa, L.C., 2012. Effects of injection parameters and EGR on combustion and emission characteristics of rapeseed oil and its blends in diesel engines. Fuel 98, 15–28.
Li, Song, et al., 2020. Effects of fuel properties on combustion and pollutant emissions of a low temperature combustion mode diesel engine. Fuel 267, 117123.
Lilik, Gregory K., Boehman, André L., 2011. Advanced diesel combustion of a high cetane number fuel with low hydrocarbon and carbon monoxide emissions. Energy Fuels 25 (4), 1444–1456.
Liu, J., Dumitrescu, C.E., 2019. Methodology to separate the two burn stages of natural-gas lean premixed-combustion inside a diesel geometry. Energy Convers. Manage. 195, 21–31.
Maroteaux, F., Saad, C., 2013. Diesel engine combustion modelling for hardware in the loop applications effects of ignition delay time model. Energy 57, 641–652.
Newhall, Henry K., 1968. Control of nitrogen oxides by exhaust recirculation–a preliminary theoretical study. SAE Trans. 1820–1836.
Noh, Hyun Kwon, No, Soo-Young, 2017. Effect of bioethanol on combustion and emissions in advanced CI engines: HCCI, PPC and GCI mode–a review. Appl. Energy 208, 782–802.
Ogunkunle, Oyetola, Ahmed, Noor A., 2019. A review of global current scenario of biodiesel adoption and combustion in vehicular diesel engines. Energy Rep. 5, 1560–1579.
Ohigashi, Shunichi, et al., 1971. Heat capacity changes predict nitrogen oxides reduction by exhaust gas recirculation. SAE Trans. 31–41.
Ong, H.C., Mahlia, T.M.I., Masjuki, H.H., 2011. A review on energy scenario and sustainable energy in Malaysia. Renew. Sustain. Energy Rev. 15 (1), 639–647.
Pachiannan, Tamilselvan, et al., 2019. A literature review of fuel effects on performance and emission characteristics of low-temperature combustion strategies. Appl. Energy 251, 113380.
Pandian, M., Sivapirakasam, S.P., Udayakumar, M., 2010. Investigations on emission characteristics of the pongamia biodiesel–diesel blend fuelled twin cylinder compression ignition direct injection engine using exhaust gas recirculation methodology and dimethyl carbonate as additive. J. Renew. Sustain. Energy 2 (4), 043110.
Qi, Donghui, et al., 2011. Effect of EGR and injection timing on combustion and emission characteristics of split injection strategy DI-diesel engine fueled with biodiesel. Fuel 90 (5), 1884–1891.
Rakopoulos, Dimitrios C., et al., 2017. Comparative evaluation of ethanol, n-butanol, and diethyl ether effects as biofuel supplements on combustion characteristics, cyclic variations, and emissions balance in light-duty diesel engine. J. Energy Eng. 143 (2), 04016044.
Ramos, J.I., 1989. Internal Combustion Engines Modeling. Hemisphere Publishing Corporation, New York.
Rashedul, H.K., et al., 2014. The effect of additives on properties, performance and emission of biodiesel fuelled compression ignition engine. Energy Convers. Manage. 88, 348–364.
Saiteja, Pajarla, Ashok, B., 2021. A critical insight review on homogeneous charge compression ignition engine characteristics powered by biofuels. Fuel 285, 119202.
Saito, Takeshi, et al., 1986. Effects of combustion chamber geometry on diesel combustion. SAE Trans. 793–803.
Shim, Euijoon, Park, Hyunwook, Bae, Choongsik, 2020. Comparisons of advanced combustion technologies (HCCI, PCCI, and dual-fuel PCCI) on engine performance and emission characteristics in a heavy-duty diesel engine. Fuel 262, 116436.
Song, H., et al., 2021. Comparisons of NO emissions and soot concentrations from biodiesel-fuelled diesel engine. Fuel 96, 446–453.
Srihari, S., Thirumalini, S., Prashanth, K., 2017. An experimental study on the performance and emission characteristics of PCCI-DI engine fuelled with diethyl ether-biodiesel-diesel blends. Renew. Energy 107, 440–447.
Sun, Y., Wang, H., Yang, C., Wang, Y., 2017. Development and validation of a marine sequential turbocharging diesel engine combustion model based on double wiebe function and partial least squares method. Energy Convers. Manage. 151, 481–495.
Suresh, M., Jawahar, C.P., Richard, Arun, 2018. A review on biodiesel production, combustion, performance, and emission characteristics of non-edible oils in variable compression ratio diesel engine using biodiesel and its blends. Renew. Sustain. Energy Rev. 92, 38–49.
Tong, Agnes S.F., et al., 2007. Renewable energy generation by full-scale biomass gasification system using agricultural and forestal residues. Pract. Period. Hazard. Toxic Radioact. Waste Manage. 11 (3), 177–183.
Wei, Jiangjun, Wang, Yuncheng, 2021. Effects of biodiesels on the physicochemical properties and oxidative reactivity of diesel particulates: A review. Sci. Total Environ. 147753.
Woschni, G., 1967. A Universally Applicable Equation for the Instantaneous Heat Transfer Coefficient in the Internal Combustion Engine. SAE Technical Paper No. 670931.
Yasar, Halit, et al., 2008. Double-wiebe function: an approach for single-zone HCCI engine modeling. Appl. Therm. Eng. 28 (11–12), 1284–1290.
Yeliana, Yeliana, et al., 2011. Estimation of double-wiebe function parameters using least square method for burn durations of ethanol-gasoline blends in spark ignition engine over variable compression ratios and EGR levels. Appl. Therm. Eng. 31 (14–15), 2213–2220.
Yousefi, Amin, Guo, Hongsheng, Birouk, Madjid, 2018. An experimental and numerical study on diesel injection split of a natural gas/diesel dual-fuel engine at a low engine load. Fuel 212, 332–346.
Zheng, Ming, Li, Tie, Han, Xiaoye, 2015. Direct injection of neat n-butanol for enabling clean low temperature combustion in a modern diesel engine. Fuel 142, 28–37.
Zheng, Ming, et al., 2008. Biodiesel engine performance and emissions in low temperature combustion. Fuel 87 (6), 714–722.
Zhu, Haoyue, et al., 2014. Effect of biodiesel and ethanol on load limits of high-efficiency premixed low-temperature combustion in a diesel engine. Fuel 106, 773–778.